J. Fluid Mech. (2006), *vol.* 551, *pp.* 1–17.
doi:10.1017/S0022112005008268 Printed in the United Kingdom

Creeping flow around a finite row of slender bodies in close proximity

By EFRATH BARTA AND DANIEL WEIHS

Faculty of Aerospace Engineering, Technion, Haifa 32000, Israel

(Received 27 January 2004 and in revised form 23 March 2005)

The flow through and around a finite row of parallel slender bodies in close proximity moving in a viscous incompressible fluid is studied. The motion occurs under creeping flow ($Re \ll 1$) conditions. This row is a model of a comb-wing configuration found in insects of the Thrips family and being developed for use for flying vehicles of mm size, operating in the creeping flow regime. We show here that such wings utilize viscous effects to carry along enough fluid to approximate continuous surfaces. The comb is described as a row of rod-like ellipsoids of slenderness ratio smaller than 0.01 at distances apart of order 10 times the minor axis and the flow field is computed by distributing singularities along the major axes of the ellipsoids. Results for the drag on the individual rods, as well as for the full row are presented. It is shown that above a certain number of rods, dependent on the geometric parameters of the comb, the row acts very much like a continuous surface, with over 95 % of the flow moving around, and not through the comb. This allows a potential saving of tens of percents in wing weight. Parametric results for number of rods, rod density (ratio of inter-rod distance to rod length) and slenderness ratio are presented demonstrating the dependence of the flow field on the configuration. It is found that 50–80 rods are required to approach the asymptotic limit of large number of rods, for various combinations of rod parameters with inter-rod distances of order of the cross-section diameter.

1. Introduction

The Stokes approximation for low-Reynolds-number flows (creeping flow) has been very successful and useful in describing the flow phenomena occurring under these conditions, which in air or water usually mean very small bodies moving at low speeds (Happel & Brenner 1973 for example). However, the slow decay of boundary effects has resulted in serious difficulties in analysing problems in which multiple bodies are involved.

Recent developments in microelectronics and power supply technology enable the design of extremely small flying vehicles, with wingspan of $O(10^{-3}\,\mathrm{m})$. Such vehicles move at speeds of up to $O(10^{-1}\,\mathrm{m\,s^{-1}})$, thus approaching the Stokes flow regime. One of the cardinal problems in designing such minuscule vehicles is weight (mass). This constraint caused us to look for weight-reducing options, leading to the idea of utilizing the slow decay of boundary effects in Stokes flow by building non-continuous comb-like structures as aerodynamic surfaces. Such comb-like surfaces will act as full wings as the fluid in the spaces between the solid parts will presumably be dragged along, and oncoming flow will be deflected around the structure. Comb-wings of this

form are found in the insect order of Thysanoptera (Thrips), insects with wingspan of 10^{-3} m or less.

Recently, the second author and colleagues showed experimentally that for miniature vehicles moving in the low-Reynolds-number (Re) range, the aerodynamic surfaces do not have to be continuous to produce the aerodynamic lift required. This was done by first manufacturing what is essentially an artificial dandelion seed, and showing that the deceleration obtained by a porous web is equivalent to that of a continuous surface (Zussman, Yarin & Weihs 2002). Next, a platform with wings formed of a comb-like array of rods was built (Naveh *et al.* 2003). Such a configuration can save up to 80 % of the wing weight, while producing lift roughly equal to a continuous wing of the same dimensions. Sunada *et al.* (2002) showed that even for $Re = 10$, comb-wings can produce 80–90 % of the forces produced by a solid surface of the same dimensions.

While insects fly by flapping and rotating their wings, the present model of uniform flow over the array of rods describes a mechanical system using just heave and a feathered recovery stroke of comb-wings, thus simplifying the mechanical transmission of forces. Future work has been initiated to analyse insect flight, including the effects of the different velocity over individual rods, as well as wing rotation, clap and fling (see Ellington 1999).

A model of flow over an infinite row of cylinders exists in the literature (Tamada & Fujikawa 1957, see also Ayaz & Pedley 1999). However, assuming an infinite row forces the flow to move between rods for any given spacing value. In a finite row, when the distance between rods is small enough for viscous 'closure' the fluid approaching the comb sees a continuous surface and escapes the low-velocity and high-drag area between row members by flowing around the structure as a whole, thus justifying the continuous wing model. In this paper we present a consistent model for the creeping flow around and within a finite row of extremely elongate bodies, thus avoiding the paradoxical results of two-dimensional flow on the one hand, and the limitations of having infinite rows on the other.

The most obvious approach to tackling a Stokes flow problem with a densely packed multi-body configuration is to distribute Stokeslets either on the surfaces of all the ellipsoids (see for example Kim & Karrila 1991) or on the bodies' centrelines (see Cox 1970; Chwang & Wu 1975; Gear 1976; Johnson 1980 and many others). Sellier (1999) applied a surface distribution and formulated a Fredholm equation of the first kind that was asymptotically solved for a single slender particle. A different approach was suggested by Liron & Barta (1992): assuming that given forces and moments are exerted on the ellipsoids, the intensities of the Stokeslets (the stresses) are determined by solving integral equations which are Fredholm equations of the second kind. However, numerical solutions based on this method are lengthy, as each slender body has to be represented by many surface sub-elements. Thus, a solution for an array of many such bodies involves a huge system of equations. Moreover, the intense variations of the intensities of the Stokeslets that characterize slender bodies lead to numerical difficulties and render this approach even less attractive for the present configuration.

In this paper we present a different approach, in which singularities are distributed only on the axes of the ellipsoids, thus considerably restricting the number of the unknowns while still keeping an high degree of accuracy (as is shown *a posteriori* in § 3). The distribution of singular solutions of Stokes equations on the main axes of the slender bodies has been shown to be the most effective method to deal with Stokes flow problems where the spacing between the various components of the system is

not too small. The singularities' strength is found by equating the velocity that they induce to the given velocities of the bodies. Johnson (1980) formulated a solution for the motion of a single curved slender body in an unbounded fluid by using matched asymptotic expansions of the integrands in the integral equations resulting in Fredholm equations of the second kind for the intensities of the singularities. In doing so, he bypassed the disadvantages that the methods used till then by Cox (1970), Geer (1976) and many others had: their solutions are given as slow converging series (specifically, they use either the slow series of $1/(\ln\varepsilon)^n$ or double series of $\varepsilon^m/(\ln\varepsilon)^n$), thus involving tedious computations, and they are applicable only away from the body ends. Davis & Brenner (2001), see also their corrected version Davis (2004) applying asymptotic expansion of the integrals and not of the integrands, faced similar difficulties which are typical of infinite series, i.e. long computation time and problems of convergence. While we do not need the capability to deal with centreline curvature, we adopt the Johnson (1980) and Barta & Liron (1988) axial singularity distribution model. The advantages of this approach are its rigorous use of the various types of singularities, the uniform validity of the solution over the whole surfaces of the bodies and its computational simplicity. In contrast to previous methods, Johnson's work does not require any specific features of the geometry of the body, thus enabling extensions to other configurations. In § 2 we specify the assumptions that underlie the model and write the resultant equations. The 'axial distribution method' has not been applied previously to densely packed configurations, so that the limitations and strengths of the model are examined by an error analysis appearing in § 3. Results are presented in § 4.

2. Formulation of the model

We describe the flow field induced by a finite row of parallel, extremely slender rod-like ellipsoids of revolution immersed in an unbounded incompressible fluid moving at $Re \ll 1$ (Stokes flow). The motion can be in any direction relative to the ellipsoids. We normalize all geometric measurements with respect to half the body length. Thus, the slenderness ratio ε is defined as the maximal radius of the ellipsoid and as d is the distance between the centres of two adjacent bodies, d/ε is necessarily larger than 2. We limit ourselves to cases where $1 \gg d \gg \varepsilon$. The number of rods m can be any integer from 2 upwards, limited only by computation time. Motion of the row induces flow around and between the ellipsoids. We compute this flow field in order to determine the range of parameters (ε, d and m values) for which the ellipsoids will 'drag' the fluid between them and the flow over the whole row of slender bodies will approach that of a continuous surface.

Thus, the Stokes flow equations

$$\nabla p = \mu \nabla^2 \boldsymbol{u}, \tag{2.1}$$

$$\nabla \cdot \boldsymbol{u} = 0, \tag{2.2}$$

are solved for the velocity $\boldsymbol{u}$ and pressure p within a medium with viscosity μ where the velocities of the bodies are given. Due to the linearity of the above equations it is sufficient to solve for motions along the three orthogonal principal directions. Translation in any other direction is a linear combination of those three. We use a coordinate system tangential, normal and bi-normal to the bodies' major axes $\boldsymbol{e}_s$, $\boldsymbol{e}_n$,

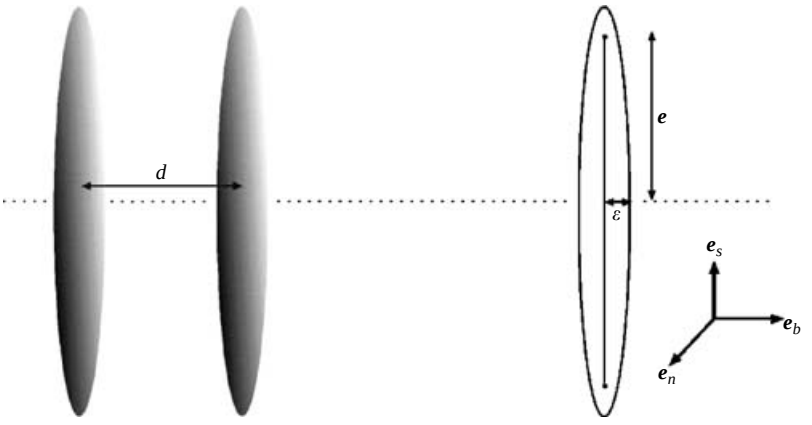

FIGURE 1. Schematic description of the configuration.

$\boldsymbol{e}_b$ (Happel & Brenner 1973). These coincide with the familiar Cartesian $\boldsymbol{e}_z$, $\boldsymbol{e}_y$, $\boldsymbol{e}_x$ axes for ellipsoids, see figure 1.

Each individual body is represented by a distribution of singularities along its axis between its foci. To leading order only Stokeslets and Doublets need to be considered (Lighthill 1975). The contribution of other types of singularities is secondary unless the bodies have significant angular velocities – cases we do not deal with. Any possible fictitious angular velocities on the individual rods, resulting from the proximity of the neighbouring rods, are cancelled by the no-slip requirement on the surfaces. Henceforth we write integral equations for the intensities of the Stokeslets by equating the given velocities v, u, w along the $\boldsymbol{e}_s$, $\boldsymbol{e}_n$, $\boldsymbol{e}_b$ directions at an arbitrary point (s, r_1, ψ) on the surface of an ellipsoid to the expressions of the velocities induced by the singularities. Using a uniformly valid asymptotic expansion, Johnson (1980) wrote integral equations of the second kind for the intensities of the Stokeslets required to describe the motion of an isolated slender spheroid. Barta & Liron (1988) have extended his solution to account for motion of two parallel bodies where the distance between their axes is comparable to the body's length, $O(1)$. In the present solution d_{ij}, the distance between the centres of ellipsoids i and j, might be as small as $O(\varepsilon)$ so the integral equations are changed to include the effect of the Doublets on adjacent bodies (which is a negligible effect where the row is sparse).

Denote by $\alpha_i^j(s)$, $\beta_i^j(s)$, respectively, the intensities of the Stokeslets and Doublets that are situated at point s on the axis of the ith ellipsoid ($i = 1, \ldots \mathrm{m}$) and act along the jth direction ($j = s, n$ or b) and define

$$e^2 = 1 - \varepsilon^2. \tag{2.3}$$

Then, assume that the relation that resulted in a uniform velocity on the surface of each of the bodies for the motion of two distant ellipsoids (Barta & Liron 1992) is valid here also, i.e. assume that

$$\beta_i^j(s) = \frac{\varepsilon^2}{2}\alpha_i^j(s)(e^2 - s^2), \quad i = 1, \ldots m, \quad j = n, s, b. \tag{2.4}$$

The velocities at point (s, r_1, ψ), i.e. at the cross-sectional plane situated at height s that has the polar coordinates (r_1, ψ), are

$$u_i(s, r_1, \psi) \cong (2L+1)\alpha_i^n(s) - \int_{-e}^{e} \frac{\alpha_i^n(s) - \alpha_i^n(s')}{|s-s'|}\,\mathrm{d}s' + \sum_{\substack{j=1\\ j\neq i}}^{m} \int_{-e}^{e} \frac{\alpha_j^n(s')}{\sqrt{(s-s')^2 + d_{ij}^2}}\,\mathrm{d}s'$$

$$+ \frac{\varepsilon^2}{2} \sum_{\substack{j=1\\ j\neq i}}^{m} \int_{-e}^{e} \frac{(e^2 - s'^2)\alpha_j^n(s')}{\sqrt{(s-s')^2 + d_{ij}^2}^3}\,\mathrm{d}s', \qquad i = 1, \ldots m, \tag{2.5}$$

$$v_i(s, r_1, \psi) \cong 2(2L-1)\alpha_i^s(s) - 2\int_{-e}^{e} \frac{\alpha_i^s(s) - \alpha_i^s(s')}{|s-s'|}\,\mathrm{d}s'$$

$$+ \sum_{\substack{j=1\\ j\neq i}}^{m} \int_{-e}^{e} \left\{ \frac{\alpha_j^b(s') d_{ij}(s-s')}{\sqrt{(s-s')^2 + d_{ij}^2}^3} \left(1 - \frac{3\varepsilon^2(e^2 - s'^2)}{2\{(s-s')^2 + d_{ij}^2\}}\right) \right.$$

$$\left. + \left(1 + \frac{(s-s')^2}{\{(s-s')^2 + d_{ij}^2\}} \left[1 - \frac{3\varepsilon^2(e^2 - s'^2)}{2\{(s-s')^2 + d_{ij}^2\}}\right]\right) \frac{\alpha_j^s(s')}{\sqrt{(s-s')^2 + d_{ij}^2}} \right\} \mathrm{d}s'$$

$$+ \frac{\varepsilon^2}{2} \sum_{\substack{j=1\\ j\neq i}}^{m} \int_{-e}^{e} \frac{(e^2 - s'^2)\alpha_j^s(s')}{\sqrt{(s-s')^2 + d_{ij}^2}^3}\,\mathrm{d}s', \qquad i = 1, \ldots m, \tag{2.6}$$

$$w_i(s, r_1, \psi) \cong (2L+1)\alpha_i^b(s) - \int_{-e}^{e} \frac{\alpha_i^b(s) - \alpha_i^b(s')}{|s-s'|}\mathrm{d}s'$$

$$+ \sum_{\substack{j=1\\ j\neq i}}^{m} \int_{-e}^{e} \left\{ \frac{\alpha_j^s(s') d_{ij}(s-s')}{\sqrt{(s-s')^2 + d_{ij}^2}^3} \left(1 - \frac{3\varepsilon^2(e^2 - s'^2)}{2\{(s-s')^2 + d_{ij}^2\}}\right) \right.$$

$$\left. + \left(1 + \frac{d_{ij}^2}{\{(s-s')^2 + d_{ij}^2\}} \left[1 - \frac{3\varepsilon^2(e^2 - s'^2)}{2\{(s-s')^2 + d_{ij}^2\}}\right]\right) \frac{\alpha_j^b(s')}{\sqrt{(s-s')^2 + d_{ij}^2}} \right\} \mathrm{d}s'$$

$$+ \frac{\varepsilon^2}{2} \sum_{\substack{j=1\\ j\neq i}}^{m} \int_{-e}^{e} \frac{(e^2 - s'^2)\alpha_j^b(s')}{\sqrt{(s-s')^2 + d_{ij}^2}^3}\,\mathrm{d}s', \qquad i = 1, \ldots m, \tag{2.7}$$

where

$$L = \ln(2/\varepsilon) \tag{2.8}$$

In equations (2.5)–(2.7) we apply the asymptotic expansion just for the body under inspection (doing so, we bypass the difficulty that the singularity presents) and not for its neighbours. For them, we simply approximate the distance between a point on the surface of the body and the axis of a neighbour by the distance between the two axes. This process is justified later: in § 3 through the *ad hoc* asymptotic analysis

(or evaluation of the errors involved with the governing equations) and in § 4 where our numerical results prove the above equations to be an acceptable approximation unless $d/\varepsilon < 5$. Our purpose is to reduce wing weight, so that denser configurations are irrelevant and not considered here.

For motion along $\boldsymbol{e}_n$ the only non-zero singularities are in this direction while motion along $\boldsymbol{e}_s$ or $\boldsymbol{e}_b$ involves singularities in both directions.

3. Evaluation of the model

The integral equations developed for two bodies that are separated by a distance of $O(1)$ were shown to be accurate within a relative error of $O(\varepsilon \ln \varepsilon)$ (Barta & Liron 1988). We now prove that the relation between the intensities of the singularities (2.4) is still optimal. The error involved in applying these integral equations is estimated afterwards.

3.1. *Asymptotic justification of the equations*

The ellipsoids are rigid bodies, so that in order to satisfy the no-slip boundary conditions, the induced velocity at point (s, r_1, ψ) must be independent of ψ. In order to get a uniformly valid asymptotic expansion we follow Johnson's (1980) method and write $\boldsymbol{u}$ far from a given singularity (outer expansion $^{(o)}$), near the singularity (inner expansion $^{(i)}$ with a stretched coordinate) and then 'tailor' both expansions by an outer–inner expansion $^{(oi)}$ (a more detailed discussion of the method appears in Johnson 1980).

For the sake of brevity we deal in this section just with three bodies which are $d = k\varepsilon$ apart ($k = O(10)$ for all practical cases) and are moving along the $\boldsymbol{e}_n$-direction. When dealing with a larger row we will have to account for the presence of the more remote bodies in the same manner as we do here for the adjacent bodies. Due to symmetry we expect just two different values of intensities: $\alpha_1(s)$ and $\alpha_2(s)$ for the edge and middle bodies respectively (the same holds for the intensities of the Doublets which are not related to the Stokeslet intensities through (2.4) at this stage of the analysis) and we explicitly write the velocity induced on the surface of the central ellipsoid.

Outer expansion:

The total velocity that Stokeslets + Doublets situated on the three axes at height s' induce at point (s, r_1, ψ) on the middle ellipsoid is

$$u^{(o)}(s, r_1, \psi; s') \cong \frac{\left(2\alpha_1^n(s') + \alpha_2^n(s')\right)}{|s - s'|} + \frac{\left(2\beta_1^n(s') + \beta_2^n(s')\right)}{|s - s'|^3} + O(\alpha\varepsilon, \beta\varepsilon). \tag{3.1}$$

Note that in the outer expansion the contribution of a singularity located at the body under consideration is identical to the contribution of the parallel point on the adjacent body.

Inner expansion:

Using a stretched coordinate σ

$$\sigma = (s - s')/\varepsilon, \tag{3.2}$$

the distance vector that connects a point located on the axis of the edge ellipsoid at height s' with (s, r, ψ) is written as

$$\boldsymbol{r} = \varepsilon[\sigma \boldsymbol{e}_s + \eta \cos\psi \boldsymbol{e}_n + (k - \eta \sin\psi)\boldsymbol{e}_b] \tag{3.3}$$

where

$$r_1 = \varepsilon\eta(s) = \varepsilon\sqrt{1-s^2} \tag{3.4}$$

and k is replaced by 0 or $-k$ in equation (3.3) when the singularity point (s') is on the middle or opposite body respectively.

The velocity induced by the six singularities (two types of singularities on the axes of three bodies) located at height s' is

$$\begin{aligned} u^i(s, r_1, \psi; \sigma) \cong\ & \frac{\alpha_1^n(s)}{\varepsilon}\left(\frac{1}{\sqrt{\sigma^2+\eta^2+k^2-2k\eta\sin\psi}} + \frac{1}{\sqrt{\sigma^2+\eta^2+k^2+2k\eta\sin\psi}}\right) \\ & + \frac{\alpha_2^n(s)}{\varepsilon\sqrt{\sigma^2+\eta^2}} + \frac{\beta_2^n(s)}{\varepsilon^3\sqrt{\sigma^2+\eta^2}^3} + \frac{\beta_1^n(s)}{\varepsilon^3}\left(\frac{1}{\sqrt{\sigma^2+\eta^2+k^2-2k\eta\sin\psi}^3}\right. \\ & \left. + \frac{1}{\sqrt{\sigma^2+\eta^2+k^2+2k\eta\sin\psi}^3}\right) \\ & + \eta^2\cos^2\psi\left[\frac{\alpha_1^n(s)}{\varepsilon}\left(\frac{1}{\sqrt{\sigma^2+\eta^2+k^2-2k\eta\sin\psi}^3}\right.\right. \\ & \left.\left. + \frac{1}{\sqrt{\sigma^2+\eta^2+k^2+2k\eta\sin\psi}^3}\right) + \frac{\alpha_2^n(s)}{\varepsilon\sqrt{\sigma^2+\eta^2}^3}\right. \\ & - \frac{3\beta_2^n(s)}{\varepsilon^3\sqrt{\sigma^2+\eta^2}^5} - \frac{3\beta_1^n(s)}{\varepsilon^3}\left(\frac{1}{\sqrt{\sigma^2+\eta^2+k^2-2k\eta\sin\psi}^5}\right. \\ & \left.\left.\left. + \frac{1}{\sqrt{\sigma^2+\eta^2+k^2+2k\eta\sin\psi}^5}\right)\right] + O(\alpha, \beta/\varepsilon^2). \end{aligned} \tag{3.5}$$

Outer–inner expansion:

Write the outer expansion by utilizing the stretched coordinate to obtain the following expression for the velocity:

$$u^{(oi)}(s, r_1, \psi; s') \cong \frac{\left(2\alpha_1^n(s') + \alpha_2^n(s')\right)}{|\varepsilon\sigma|} + \frac{\left(2\beta_1^n(s') + \beta_2^n(s')\right)}{|\varepsilon\sigma|^3} + O(\alpha, \beta/\varepsilon^2). \tag{3.6}$$

The induced velocity at (s, r_1, ψ) is a result of the contributions of all the singularities distributed between the foci of the bodies; therefore to the leading order

$$u(s, r_1, \psi) \cong \int_{-\sigma_1}^{\sigma_2} u^{(i)}(s, r_1, \psi; \sigma)\varepsilon\,\mathrm{d}\sigma + \int_{-e}^{e}\left(u^{(o)}(s, r_1, \psi; s') - u^{(oi)}(s, r_1, \psi; s')\right)\mathrm{d}s'. \tag{3.7}$$

where $\sigma_1 = (e+s)/\varepsilon$, $\sigma_2 = (e-s)/\varepsilon$.

In order to satisfy the rigid-body no-slip condition we seek a relation between $\alpha(s)$ and $\beta(s)$ that will render u ψ-independent. We specify here just the ψ-dependent

terms that we get after substitution of (3.1), (3.5) and (3.6) in (3.7):

$$\alpha_1^n(s)\int_{-\sigma_1}^{\sigma_2}\left\{\frac{1}{\sqrt{\sigma^2+\eta^2+k^2-2k\eta\sin\psi}}+\frac{1}{\sqrt{\sigma^2+\eta^2+k^2+2k\eta\sin\psi}}\right.$$
$$\left.+\eta^2\cos^2\psi\left[\frac{1}{\sqrt{\sigma^2+\eta^2+k^2-2k\eta\sin\psi}^3}+\frac{1}{\sqrt{\sigma^2+\eta^2+k^2+2k\eta\sin\psi}^3}\right]\right\}\mathrm{d}\sigma$$
$$+\eta^2\cos^2\psi\int_{-\sigma_1}^{\sigma_2}\left\{\frac{\alpha_2^n(s)}{\sqrt{\sigma^2+\eta^2}^3}-\frac{3\beta_2^n(s)}{\varepsilon^2\sqrt{\sigma^2+\eta^2}^5}\right\}\mathrm{d}\sigma$$
$$+\frac{\beta_1^n(s)}{\varepsilon^2}\int_{-\sigma_1}^{\sigma_2}\left\{\frac{1}{\sqrt{\sigma^2+\eta^2+k^2-2k\eta\sin\psi}^3}+\frac{1}{\sqrt{\sigma^2+\eta^2+k^2+2k\eta\sin\psi}^3}\right.$$
$$\left.-3\eta^2\cos^2\psi\left[\frac{1}{\sqrt{\sigma^2+\eta^2+k^2-2k\eta\sin\psi}^5}+\frac{1}{\sqrt{\sigma^2+\eta^2+k^2+2k\eta\sin\psi}^5}\right]\right\}\mathrm{d}\sigma. \tag{3.8}$$

In the case of a sparse row, out of the above three integrals we retain just the second one to leading order. This is found to be equal to

$$2\left(\frac{2\beta_2^n(s)}{\varepsilon^2(e^2-s^2)}-\alpha_2^n(s)\right)\frac{(1-s^2)\cos^2\psi}{1-e^2s^2}$$

or null when (2.4) is satisfied. In any other case, the first integral involves logarithmic expressions while the third one does not. Therefore there is no relation, be it (2.4) or any other, that yields a ψ-independent velocity. The optimal choice would be to use (2.4) as we did above but this means that the induced velocity depends on ψ to leading order through the following term (multiplied by $\alpha_1^n(s)$:

$$\ln\left\{\frac{(e-s)+\sqrt{(1-es)^2+k^2-2k\sqrt{1-s^2}\sin\psi}}{-(e+s)+\sqrt{(1+es)^2+k^2-2k\sqrt{1-s^2}\sin\psi}}\right\}$$
$$+\ln\left\{\frac{(e-s)+\sqrt{(1-es)^2+k^2+2k\sqrt{1-s^2}\sin\psi}}{-(e+s)+\sqrt{(1+es)^2+k^2+2k\sqrt{1-s^2}\sin\psi}}\right\}. \tag{3.9}$$

When k is relatively large (a sparse row) $k^2 \gg 2k\sqrt{1-s^2}\sin\psi$ and thus the above expression is, to leading order, a function of k, and s and depends on ψ just to second order: $k^2-2k\sqrt{1-s^2}\sin\psi = k^2(1+\sqrt{1-s^2}O(\psi/k)) \cong k^2$. In addition, for any value of k the ψ-dependence is very weak when $(1-s^2)$ is very small, i.e. close to the foci where $s^2 \cong 1$.

3.2. *Method of numerical solution and error analysis*

The integral equations (2.5)–(2.7) have to be solved numerically in order to compute the values of the intensities of the singularities. As Johnson suggested, the two 'intuitive' approaches are as follows. (i) An iterative solution (used by Barta & Liron 1988): under the integral sign use the current α value and simply integrate to yield the next iterative value outside the integral sign. (ii) Convert the integral equations to a system of linear equations where each integral is replaced by an appropriate summation (e.g. by the rectangle or trapezoid rule). Using the iterative approach

is simple and appealing; however it proves to be problematic for dense or large rows (where d is very small or m is large) for any initial guess (e.g. zero intensities, intensities valid for an isolated body etc.). In such cases the solution oscillates and the convergence of the oscillations to the solution depends on the initial guess. Variations of this simple method that consider combinations of couples of previously computed iterations improved the results for just some of the cases within the parameters range.

The 'linear system approach' proved to be effective for every parameters set and was therefore chosen for the solution of the integral system. The interval of integration, $2e$ is divided to sub-intervals each of ds length. The number of numerical points used depends on the parameters values of the problem (e.g. direction of motion, distances between rods, slenderness ratio etc.) but in general it does not exceed 200 points (spread evenly on the axis of each body). We validate that a change in ds will not significantly alter the results, i.e. there is convergence to the solution of the integral equations. However, as was discussed above, the integral equations involve inaccuracies (which might be non-negligible when the ellipsoids are densely packed) and we wish to estimate the effect of those inaccuracies on the solution. We apply the following well-known theorem to get an upper bound to the error of the solution, namely the error involved with solving the linear system $(A+\delta A)\,(\boldsymbol{x}+\delta\boldsymbol{x})=\boldsymbol{b}$ satisfies

$$\frac{\|\delta x\|}{\|x+\delta x\|}\leqslant K(A)\frac{\|\delta A\|}{\|A\|}. \tag{3.10}$$

$K(A)$ is the matrix condition number which was found to be of $O(10)$ for the systems we were dealing with, i.e. quite small for this size of matrix (a typical situation for stable systems like the ones originating from Fredholm equations of the second kind). In order to estimate the error, δA in constructing the matrix by our method, we compare the terms we use (the integrands that appear in (2.5)–(2.7)) assuming that the surface and axis coincide with the 'accurate terms', i.e. the values obtained for points on the surface. Using Taylor expansions gives an error of $O(\varepsilon/\mathrm{d}^2)$ for the coefficients on the ellipsoids at the edges of the row and $O(\varepsilon^2/\mathrm{d}^3)$ otherwise. This error estimation is used to compute $\|\delta A\|$ in (3.10). For the examples presented in the next section we found that the upper bound for the relative error in $\alpha(s)$, represented by the left-hand side of (3.10), is usually less than 2 %, the actual value depending on the specific chosen vector norm, on ds (the length of the integration subintervals), on the direction of motion and mainly on the values of the parameters m, ε and d. In any case the convergence of the numerical solution to the 'real' solution is assured since the matrices are verified to be positive definite.

We have no way of estimating the accuracy of the solution process *a priori* but we may validate it *a posteriori* by

(i) Comparing with known solutions – the solutions here do indeed tend to previous solutions for the case of two relatively distant ellipsoids (Barta & Liron 1988).

(ii) For motions along the tangential or bi-normal directions verifying that the secondary intensities computed at the centres of the ellipsoids (which should be zero by symmetry considerations) are extremely small.

(iii) Computing the induced velocity on the surfaces of the bodies to check whether it coincides with the dictated no slip value. Specifically, we compute $\boldsymbol{u}(s, r_1, \psi)$ for various points on the surface of any of the ellipsoids:

$$u^j(s,r_1,\psi)=\sum_{i=1}^{m}\int_{-e}^{e}\frac{\alpha_i^j(s')}{r}+\frac{\beta_i^j(s')}{r^3}+\frac{r^j\sum_k\alpha_i^k(s')r^k}{r^3}-3\frac{r^j\sum_k\beta_i^k(s')r^k}{r^5}\,\mathrm{d}s',\quad j=n,s,b, \tag{3.11}$$

where we sum k over the three orthogonal directions, $r = |\boldsymbol{r}|$ and $\boldsymbol{r}$ is the radius vector that connects point (s, r_1, ψ) and s'–the location of the singularities. Faultless solution would yield the dictated velocity at all points and the deviation from this is an indication of our errors. Note that (3.11) involves multiplication of the solution (α and β) by the inverse of the distance of the point on the surface from the axis. It thus enhances the inaccuracies at the ends of the bodies where this distance becomes extremely small. We used (3.11) to estimate the accuracy of the computed velocities and found that within the range of our parameters values, i.e. ε varies between 0.01 and 0.001, d equals (5–50)ε and the number of rods m is 10–80, the relative error for the velocity is about 1.5 % at most (for $i = 1$ or m) where $s \cong 0$ (i.e. near the centre of the ellipsoid) and is smaller in other regions of the row. The errors are expected to decrease towards the ends of the bodies, since our assumption of circumferential symmetry is more legitimate there, see (3.9). The errors arising in the determination of the intensities of the singularities are probably (there is no way to verify this) higher and the high accuracy obtained here in the computation of the velocities is an outcome of the integration in (3.11) which averages the local inaccuracies. Since the computation of the drag involves integration as well (see equation (4.1) below) we deduce that the two relevant quantities, velocity and drag, are computed with satisfactory accuracy.

Based on the above error analysis and on many numerical examinations we can justify the claim that the velocities that we compute for any point within the central part of the fluid are usually accurate to within 1 % error. Increasing m, the number of bodies in the array, and/or increasing the gaps between the bodies and/or using more-slender bodies reduces the errors involved.

4. Results

Equations (2.5)–(2.7) were converted to a system of linear equations and were solved yielding the distribution of the intensities of the Stokeslets for values of the parameters that are characteristic of the physical/biological situations described in the Introduction. Henceforth we concentrate on the physically relevant properties such as the total drag acting on each body, which is a measure of the blocking effect of the row, and the flow field in the vicinity of the bodies. In the following we deal with the drag forces on the array of rods in different directions. These are the equivalent to lift on a body with comb-wings, when the wing motion is vertically downwards, as the flow is forced downwards, reacting upwards on the body.

4.1. *Drag*

Assuming that the bodies move along each of the three orthogonal directions $\boldsymbol{e}_s$, $\boldsymbol{e}_n$, $\boldsymbol{e}_b$ with unit velocity, the drag exerted on the ith ellipsoid is given by

$$D_i^j = 8\pi\mu \int_{-e}^{e} \alpha_i^j(s)\,\mathrm{d}s, \quad j = n, s, b, \quad i = 1, \ldots . m. \tag{4.1}$$

Note that the drag always has a component in the direction of motion only. Although motion along the tangential or bi-normal directions involves stresses along the other direction as well, these stresses are asymmetric with respect to the centre of the body and do not contribute to the total drag on each body. Those secondary stresses are relatively small. For example, in a row of 10 ellipsoids with $d = 10\varepsilon$ and $\varepsilon = 1/300$ moving in the $\boldsymbol{e}_b$-direction, the ratio between the maximum local stresses in the $\boldsymbol{e}_s$- and $\boldsymbol{e}_b$-directions, attained at the foci of the first or last body, is 0.16. Along the major part of the axis the secondary intensities are much smaller in comparison to

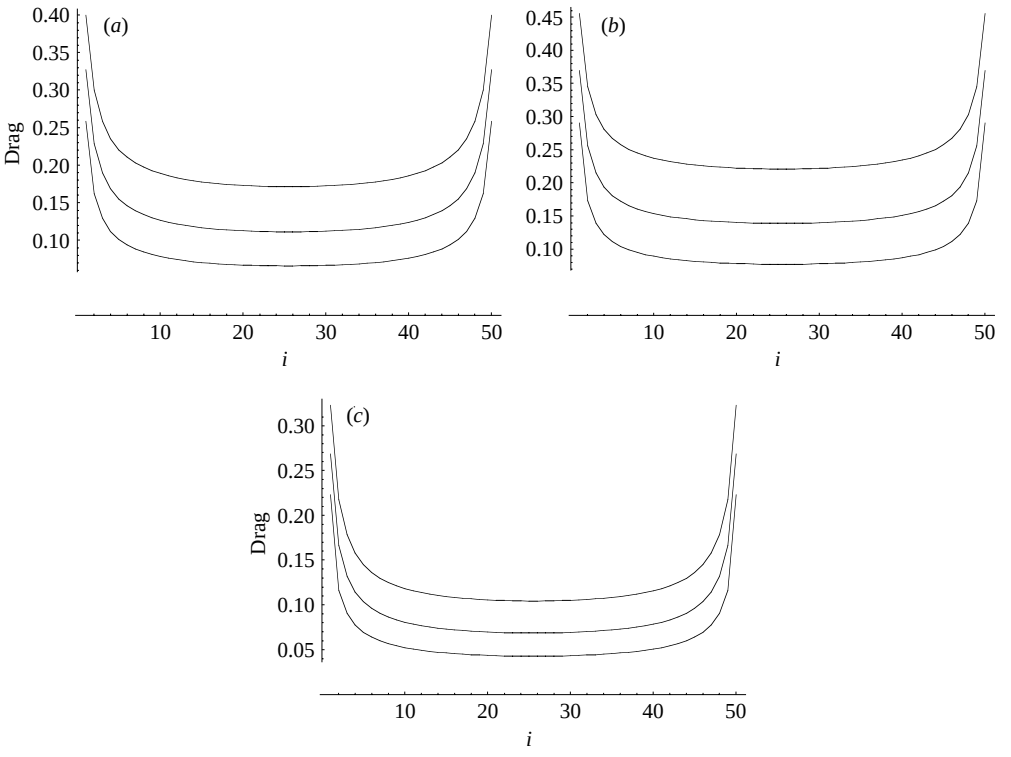

FIGURE 2. The total drag, normalized by the drag for an isolated ellipsoid, on each of the ellipsoids within a row of 50 bodies moving in the normal direction for $\varepsilon = 1/300$. $d = 50\varepsilon$ (top curve), $d = 25\varepsilon$ (middle) and $d = 10\varepsilon$ (bottom). Motion in (*a*) normal (*b*) tangential and (*c*) bi-normal directions.

the 'main' intensities, decreasing to zero at the centres. The secondary intensities set up a moment on each body. For motion in the $\boldsymbol{e}_s$-direction this means that bodies on opposite sides within the row tend to tilt in opposite directions so as to increase the spacing between their 'heads'. The sum of all the moments is null due to the asymmetry with respect to the centre of the row.

Figure 2 displays the distribution of the drag force exerted on the various ellipsoids normalized by the drag for a single ellipsoid as obtained by Chwang & Wu (1975) for motions along the three orthogonal directions. Obviously, the presence of adjacent bodies moving in the same direction lower the drag exerted on the body since they induce a flow within the surrounding fluid so that each body is actually immersed in a fluid that flows in the direction of its motion. The closer the ellipsoid is to the centre of the row, the lower the drag exerted on it due to the effect of the near-by ellipsoids, which is highest there. The most prominent interaction occurs when the motion is along the bi-normal direction (i.e. in the plane of the rods, perpendicular to the major axes) while the least significant one occurs in motion along the tangential direction, in accordance with the results for two bodies (Barta & Liron 1988). Hence, the smallest drag forces are found for motion along the bi-normal direction, see figure 2. The sum of all the forces exerted on the bodies is presented in table 1. The higher the interactions between the bodies are, the less force is needed in order to make the row move, therefore a denser row involves reduced total drag compared to a sparser

	$d=10\varepsilon$	$d=25\varepsilon$	$d=50\varepsilon$
$\boldsymbol{e}_s$-direction	5.0	8.3	12.5
$\boldsymbol{e}_n$-direction	4.4	6.9	10.1
$\boldsymbol{e}_b$-direction	3.1	4.6	6.5

TABLE 1. The overall drag forces exerted on a row of 50 ellipsoids with $\varepsilon=1/300$ moving along the three orthogonal directions for various gaps d, normalized by the drag on a single ellipsoid.

	$d=10\varepsilon$	$d=25\varepsilon$	$d=50\varepsilon$
$\boldsymbol{e}_s$-direction	3.4	5.1	7.3
$\boldsymbol{e}_n$-direction	3.2	4.5	6.2
$\boldsymbol{e}_b$-direction	2.4	3.2	4.2

TABLE 2. As table 1 but with $\varepsilon = 1/1000$.

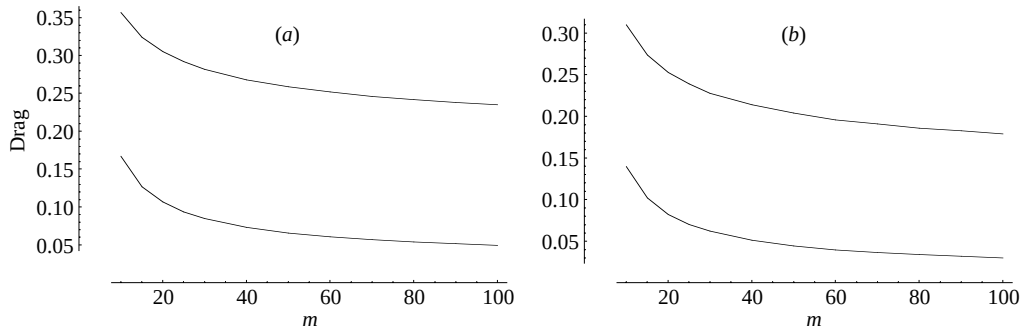

FIGURE 3. The total drag exerted on ellipsoids on the edge and in the centre of a row (top and bottom curves respectively) moving along the normal direction as a function of m, $10 \leqslant m \leqslant 100$, $d=10\varepsilon$. (a) $\varepsilon=1/300$, (b) $\varepsilon=1/1000$.

one and motion in the $\boldsymbol{e}_b$-direction involves reduced total drag compared to motion along the other directions.

Next we look at the effect of varying the slenderness ratio. Note that by fixing m and the ratio d/ε but changing ε we actually change the 'aspect ratio' of the whole row, i.e. we change the ratio between its total length and width. We expect that reducing ε or the total span of the row will result in reduced overall drag. Comparison of tables 1 and 2 demonstrates this. Moreover, it shows that wherever the interactions are more significant, the sensitivity with respect to ε is lower (because then even ε as high as $1/300$ is small enough as to be very effective), e.g. when $d=10\varepsilon$ the overall drag for ε=1/1000 is 77 % and 68 % of the overall drag for $\varepsilon=1/300$ for motions along the $\boldsymbol{e}_b$- and $\boldsymbol{e}_s$-directions respectively.

Figure 3 shows the dependence of the drag on m. The more ellipsoids we add to the row, the lower the drag exerted on each body becomes. For $\varepsilon=1/300$ this monotonic dependence reaches an asymptotic value in motion along the normal direction when $m \cong 80$, indicating that extending a 'wing' composed of a row of slender rods results in diminishing returns beyond a certain limiting number of rods. Reduction of ε involves more intense dependence of the drag on m thus slightly increasing the asymptotic m value (compare figures 3a and 3b). This form of dependence of the drag on m

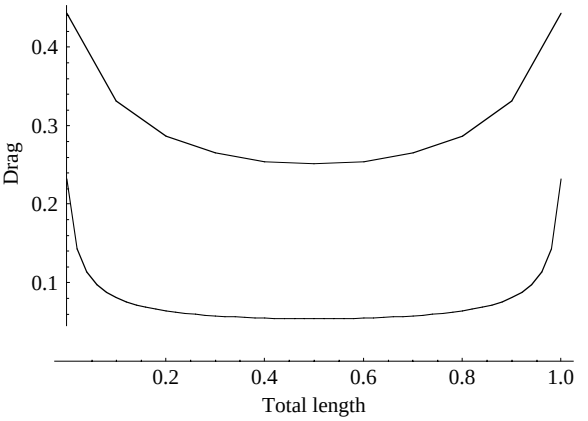

FIGURE 4. The total drag exerted on ellipsoids within a row of length 1 moving in the normal direction for $\varepsilon = 1/500$. $m = 11$ and $d = 50\varepsilon$ (top curve) or $m = 51$ and $d = 10\varepsilon$ (bottom).

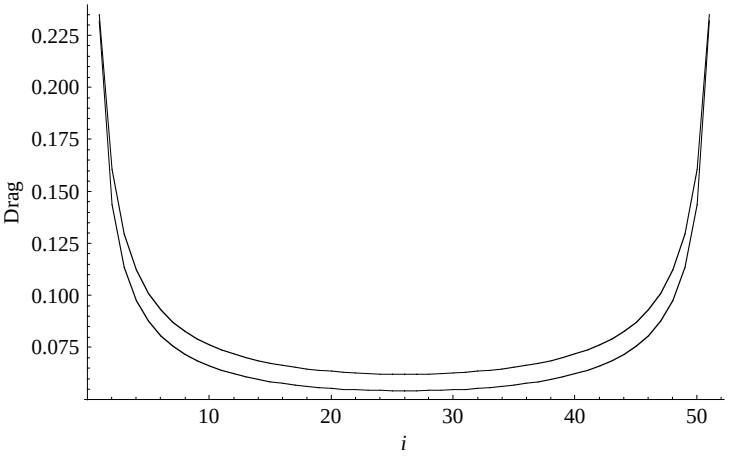

FIGURE 5. The total drag on each of the ellipsoids within a row of 51 bodies moving in the normal direction for $\varepsilon = 1/1500$, $d = 30\varepsilon$ (top curve) and $\varepsilon = 1/500$, $d = 10\varepsilon$ (bottom).

is found for motion in the other directions with slightly different numerical values. While figure 3 presents the effect of extending a given row, figure 4 presents the effect of increasing m but keeping the same span, i.e. increasing density of the row. The more ellipsoids contained in a given space, the lower is the drag on each of them. Moreover, the densely packed situation is characterized by almost homogeneous drag throughout the row (except for the few ellipsoids on the edges) while the variations between the bodies in the 'sparsely packed situation' are considerable. Figure 5 shows the minor effect of changing the slenderness ratio. Replacing the ellipsoids in a given row by ellipsoids that are three times more slender results in slightly less pronounced interactions (therefore, only slightly higher drag forces).

4.2. *Velocities*

Another important outcome of the model is the velocity of the fluid that surrounds the ellipsoids. Using (3.11) we can compute the velocity anywhere, but in order to get an indication of whether the row actually acts like a continuous surface it is sufficient

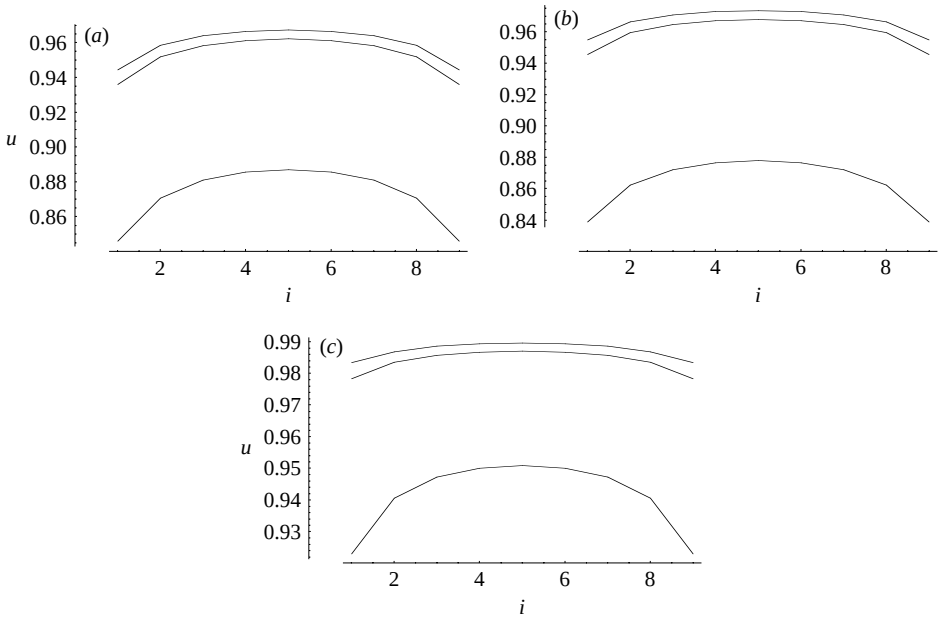

FIGURE 6. The velocities at the midpoints between the ellipsoids at heights: $s = 0$, $s = 0.5e$, $s = 0.95e$ (from top downwards) where $m = 10$, $\varepsilon = 1/300$ and $d = 10\varepsilon$. Motion in (a) normal, (b) tangential and (c) bi-normal directions.

to compute velocities in the middle of the gaps between the bodies, the midpoints, where we expect the local minimum velocity.

Figure 6 presents those velocities for a row of 10 slender ($\varepsilon = 1/300$) ellipsoids where $d = 10\varepsilon$. In a way, this figure demonstrates the same trends as in figure 2, namely: closer to the centre of the row the interactions are higher (thus the low drag and the high velocity of the fluid); the highest interactions occur in motion along the bi-normal direction while the lowest interactions occur in motion along the tangential direction. However, the drag computation provides global information only, while the fluid velocity is a local phenomenon that sheds more light on the situation. Comparing the velocities at three positions along the length of the rods, it is clear that a uniform velocity is obtained over most of the comb and the only significant change occurs near the ends of the bodies (approximately 10 % of the length). This result is explained when one considers the solutions computed for the Stokeslets' intensities – it turns out that for each ellipsoid which is not on the edge $\alpha(s)$ is almost constant along the major part of the axis and then steeply increases towards the foci of the body, see figure 7. Moreover, the variation of $\alpha(s)$ from one body to the next is minor for most of the row (significant changes just near the boundaries for the one or two end ellipsoids). The velocities at any given location are affected mainly by the singularities at this location (and its near surroundings) and therefore will obey the same rules as the local intensities.

Figure 8 shows the effect of extending the row on the fluid velocity between the rods (i.e. the remaining porosity). Note the difference between the situation presented in figure 3(a) where we concluded that the asymptotic value of m should be about 80, and the present situation where for the same d and ε values the fluid flows with the ellipsoids for most of the row when $m \geqslant 50$. Further extension would increase the velocity of the fluid a little; however the deviation from a coherent motion for the central portion of the row is already within the limits of accuracy for $m = 50$. This

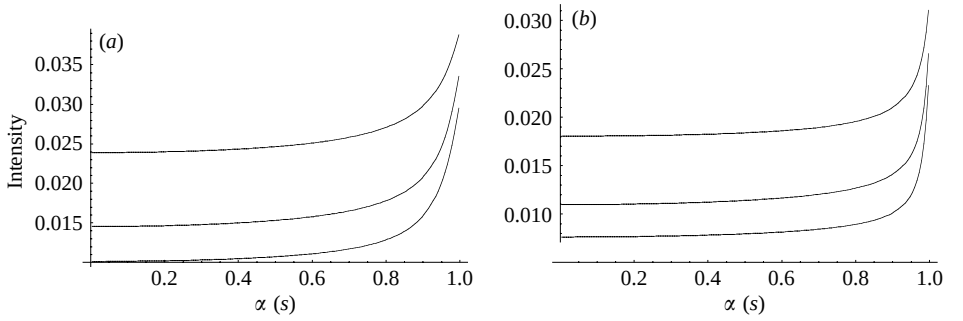

FIGURE 7. The distribution of intensities of Stokeslets along the half-axis of the first (top curve), second (middle curve) and middle ellipsoid (bottom curve) for a motion in the normal direction where $m = 10$ and $d = 10\varepsilon$. (*a*) $\varepsilon = 1/300$, (*b*) $\varepsilon = 1/1000$.

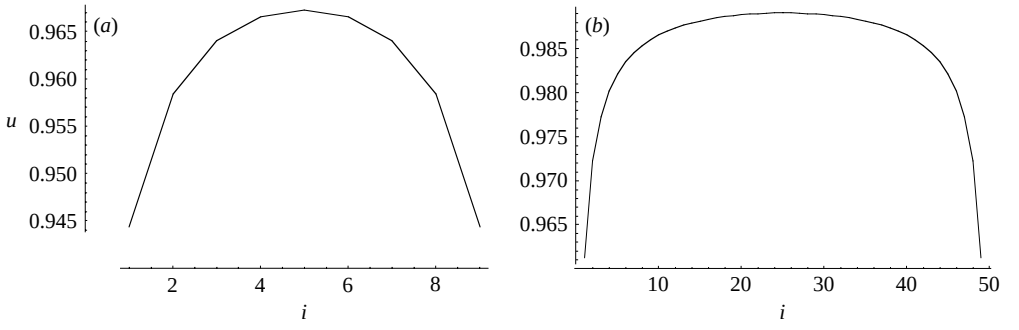

FIGURE 8. The velocity in the normal direction at the midpoints between slender ellipsoids $\varepsilon = 1/300$, $d = 10\varepsilon$, $s = 0$ (the equatorial plane) for (*a*) $m = 10$ and (*b*) $m = 50$.

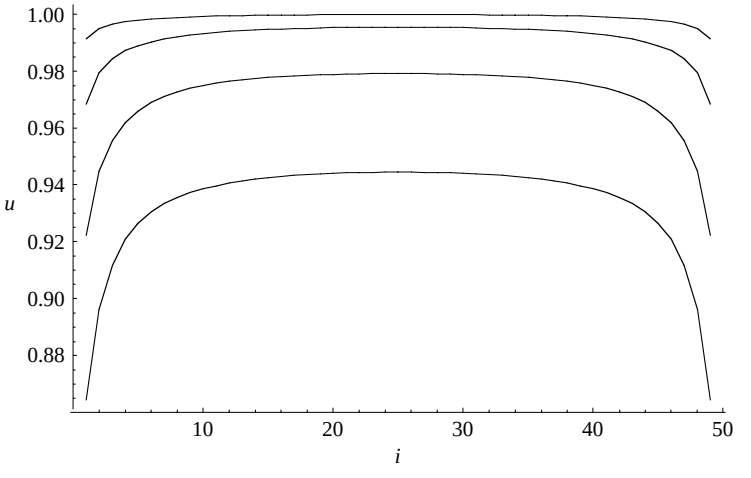

FIGURE 9. The velocity in the normal direction at the midpoints between the ellipsoids at $s = 0$ (the equatorial plane) for $m = 50$, $\varepsilon = 1/300$. $d = 5\varepsilon$, 10ε, 25ε, 50ε (from top to bottom).

difference is probably due to the fact that increasing m has much more pronounced effect at the tips of the ellipsoids than near their centres.

Figure 9 shows that a row of 50 ellipsoids acts as a continuous wing for all practical purposes when $d \leqslant 25\varepsilon$. While the top curve is not fully justified theoretically, the results are consistent, pointing to the robustness of the model. Further increasing of

the gaps between the bodies induces a non-uniform velocity; the fluid lags a little behind the ellipsoids in the central area of the row and lags even more towards the ends. When $d = 50\varepsilon$ further extension of the row (higher m values) will result in a more homogenous fluid velocity across the row, but the fact that the fluid lags behind the ellipsoids will not change, e.g. increasing m from 50 to 80 will raise the maximum resultant velocity along the normal direction just slightly (from 0.937 to 0.944, equivalent to a porosity of 6.3–5.6 %). In other words, the most effective way to approach a continuous surface is to reduce the distance between rods d. Increasing the number of rods m will have a secondary effect and decreasing their slenderness ratio ε will be even less effective.

5. Discussion

We have calculated the creeping flow field in the vicinity of a row of slender ellipsoids moving in any given arbitrary direction within a stationary medium. Using an axial distribution of singularities proved to be surprisingly accurate and enabled us to solve for the drag forces exerted on the bodies and for the velocity induced in their surroundings with a relatively low computational effort. We found that the axial distribution of Stokeslets and Doublets presented here produces the best results. We checked the possibility of distributing Quadrupoles and Stresslets as well. Johnson (1980) proved that the accuracy of the solution for an isolated ellipsoid would improve after distributing Stresslets and Quadrupoles with intensities of $O(\alpha\varepsilon^2)$ and $O(\alpha\varepsilon^4)$ respectively. For the present configuration using such singularities might improve the circumferential asymmetry by $O(\alpha\varepsilon)$ at most (while the required correction is of $O(\alpha)$). The option of using higher intensities is excluded because it would interfere with the circumferential symmetry that the singularities induce on 'their own ellipsoid'. Limitations on the accuracy of the method of axial distribution are expected due to the assumption of symmetrical flow around each ellipsoid. This assumption is inherent to the method but is physically inaccurate. We analysed the implications of this assumption and showed them to be very minor even for a dense row.

Other solutions, such as Tamada & Fujikawa (1957) and Ayaz & Pedley (1999) who dealt with an infinite row of infinitely long cylinders, are not comparable, as the fluid cannot 'escape' around the row as in the present case of finite rows, but has to 'find its way' within densely packed bodies. In our case, reducing the distance d between rods results in a very low shear gradient (as the fluid is being dragged with the bodies). Therefore, the infinite row case is not the limit of the finite configuration for $m \to \infty$ but is a different situation entirely. We see that:

(i) The presence of additional bodies has a very significant effect on the drag and it is important even if the bodies are far away (e.g. in figure 2 the drag forces are smaller than half of their isolated-body value even when the inter-body distance equals 50 radii. See also tables 1 and 2)

(ii) The drag depends on both the total span of the row and the density of the row (figures 3 and 4).

(iii) The more slender the bodies, the less pronounced are the interactions between the bodies (figure 5).

Qualitatively similar results were obtained by Cheer & Koehl (1987), who studied the case of motion of two cylinders.

Our ability to predict ranges of the parameters values for which a row of slender ellipsoids behaves like a continuous surface can be an important tool in designing of minimum-weight wings for minuscule flying or swimming vehicles. Thus, for mm-sized

small flying vehicles, wings of solidity ratio of around 10:1 will supply approximately 90 % of the force produced by a solid surface as the normal drag, which represents the loss of aerodynamic force by leakage, is less than 10 % (see bottom curve of figure 2*a*). This wing weighs only one–tenth of the weight of the wing with continuous surface, i.e. a nine-fold increase in the force/weight ratio is obtained!

REFERENCES

Ayaz, F. & Pedley, T. J. 1999 Flow through and particle interception by an infinite array of closely-spaced circular cylinders. *Eur. J. Mech.* B/*Fluids* **18**, 173–196.

Barta, E. & Liron, N. 1988 Slender body interactions for low Reynolds numbers – Part II: Body-body interactions. *SIAM J. Appl. Maths* **48**, 1262–1280.

Cox, R. G. 1970 The motion of long slender bodies in a viscous fluid. Part 1: general theory. *J. Fluid Mech.* **44**, 791–810.

Chwang, A. T. & Wu, T. Y. 1975 Hydromechanics of low-Reynolds-number flow. Part 2. Singularity method for Stokes Flow. *J. Fluid Mech.* **67**, 787–815.

Cheer, A. Y. L. & Koehl, M. A. R. 1987 Paddles and rakes: fluid flow through bristled appendages of small organisms. *J. Theor. Biol.* **129**, 17–39.

Davis, A. M. J. 2004 Limitation on the use of slender-body theory in Stokes flow: Falling needle viscometer errata. *Phys. Fluids* **16**, 4204–4205.

Davis, A. M. J. & Brenner, H. 2001 The falling needle viscometer. *Phys. Fluids* **13**, 3086–3088.

Ellington , C. P. 1999 The novel aerodynamics of insect flight: applications to micro-air vehicles. *J. Expl Biol.* **202,** 3439–3448.

Geer, J. 1976 Stokes flow past a slender body of revolution. *J. Fluid Mech.* **78**, 577–600.

Happel, J & Brenner, H. 1973 *Low Reynolds Number Hydrodynamics*. Noordhoff.

Johnson, R. E. 1980 An improved slender-body theory for Stokes flow. *J. Fluid Mech.* **99** 411–431.

Kim, S. & Karrila, S. J. 1991 *Microhydrodynamics: Principles and Selected Applications*. Butterworth-Heinemann.

Lighthill, J. 1975 *Mathematical Biofluiddynamics*. SIAM Regional Conference Series in Applied Mathematics, vol. 17.

Liron, N. & Barta, E. 1992 Motion of a rigid particle in Stokes flow: a new second-kind boundary-integral equation formulation. *J. Fluid Mech.* **238**, 579–598.

Naveh, R., Yechieli, R., Sachyani, M. & Weihs, D. 2003 MEMS based structure for miniature aerial system. ISRAMEMS 2003, Tel Aviv, Nov. 2003.

Sellier, A. 1999 Stokes flow past a slender particle. *Proc. R. Soc. Lond.* A **455**, 2975–3002.

Sunada, S., Takashima, H., Hattori, T., Yasuda, K. &. Kawachi, K. 2002 Fluid-dynamic characteristics of a bristled wing. *J. Expl Biol.* **205**, 2737–2744.

Tamada, K. & Fujikawa, H. 1957 The steady two-dimensional flow of viscous fluid at low Reynolds numbers passing through an infinite row of equal parallel circular cylinders. *Q. J. Mech. Appl. Maths* **10,** 426–432.

Zussman, E., Yarin, A. L. & Weihs, D. 2002 A micro-aerodynamic decelerator based on permeable surfaces of nanofiber mats. *Exps. Fluids* **33**, 315–320.